atoms

MDPI

Article

Doubly and Triply Differential Cross Sections for Single Ionization of He by Fast Au^{53+} Using a Multi-Body Quasiclassical Model

François Frémont

Centre Interdisciplinaire de Recherche sur les Ions, la Matière et la Photonique, Université de Caen-Normandie, 6 bd du Maréchal Juin, 14050 Caen CEDEX, France; francois.fremont@ensicaen.fr; Tel.: +33-658057482

Received: 17 February 2020; Accepted: 2 May 2020; Published: 6 May 2020

Abstract: A multi-body multi-center quasiclassical model was used to determine doubly- and triply-differential cross sections following single ionization in 3.6 MeV/amu Au^{53+} + He collisions. The present model improved recent calculations, in which free electrons were added in the collision to reproduce, at least qualitatively, the experimental binary peak. In the present calculations, the electrons, that were assumed to originate from the collisions of Au^{53+} with surfaces before colliding with the He target, were now considered to be in the field of the projectile, with nearly the same velocity. The agreement between the calculations and the experiment was improved, for both the doubly- and the triply-differential cross sections and was better than previous calculations based on quantum mechanics.

Keywords: ion-atom collisions; ionization; classical trajectory Monte Carlo (CTMC) calculations; fully differential cross sections

1. Introduction

During the last two decades, considerable theoretical work has been performed to analyze single-ionization (SI) following 3.6 MeV Au^{53+} + He collisions, for which the strong interaction between the outgoing projectile, the residual ionized He^+ target and the emitted target electron requires sophisticated treatments. The doubly differential cross sections (DDCS) $d^2\sigma_{SI}/dq_\perp dE_e$, where $\vec{q_\perp}$ is the transverse momentum transfer of Au^{53+} and E_e is the emitted electron energy, were calculated using classical [1,2] and quantum [3–5] mechanics methods. Whatever the degree of sophistication, the theoretical models were not able to reproduce neither the absolute magnitude of the experimental DDCS that were determined experimentally, nor to reveal the presence of the binary peaks that were observed at E_e larger than 50 eV and for large values of $q_\perp$ [3]. Similarly, for the triply differential cross sections (TDCS), the theoretical cross sections [6–12] $d^3\sigma_{SI}/dq_\perp dE_e d\Omega_p$, where $d\Omega_p = 2\pi \sin\theta_p d\theta_p$ and θ_p is the scattering angle of the projectile, were also found to deviate noticeably from the experimental results [6,7].

Recently, we performed new calculations using four-body classical trajectory Monte Carlo (4B-CTMC) calculations to analyze DDCS following 3.6 MeV Au^{53+} + He collisions [13]. Even though our calculations did not reproduce the experimental binary peaks, the overall agreement was considerably improved by introducing a large amount of electrons as projectiles [13]. That preliminary calculation was conducted using free electrons, i.e., electrons that do not interact with the ion projectile or among them. To explain the presence of such electrons, we hypothesized that they may be produced in collisions between Au^{53+} and surfaces (for example collimators) before entering the collision zone. Despite the presence of the magnetic field $\vec{B}$ in the experimental setup (whose value was of the order of 20 Gauss) that in principle deviates spurious electrons, convoy electrons with a velocity close to

the projectile velocity (12 a.u.) remained close to the ion projectile, with an helicoidal trajectory, since the Coulombic interaction between the electrons and Au^{53+} was much stronger than that between the electrons and $\vec{B}$.

Firstly, we assumed that the convoy electrons were randomly produced at a distance z_e in the range 0–50 a.u. from the ion projectile. It should be noted that the distance of 50 a.u. was chosen arbitrarily since no detailed information exists on this distance. However, it was verified, for distances varying from 20 to 200 a.u., that the shape of the final distributions (presented in the next section) was quite unchanged. At time t = 0, the distance r_e between an electron and the projectile axis is at maximum a few a.u. Therefore, the convoy electrons were assumed to be in a cylinder of length z_e and of base radius r_e. The time evolution of the r_e distribution is presented in Figure 1, for a total number of initial convoy electrons of 10,000 in order to obtain good statistics and assuming no interaction between the convoy electrons. Due to the presence of $\vec{B}$, r_e increased with time. Nevertheless, even at t = 10^8 a.u., i.e., after 60 cm collision distance, the distribution maximum was located between 10^{-6} cm and 10^{-2} cm, which was much smaller than the width of the target jet, so that most of the convoy electrons were able to reach the target within the approximation of independent convoy electrons. At this point, the question of the interaction between the convoy electrons must be discussed. Since information was missing about the convoy electron distributions, only an estimation of the possible influence of this interaction was made. Consider 200 electrons in a cylinder whose volume is of the order of 1000 a.u.^{3}. In this case, the mean distance between two electrons was about 2 a.u., inducing a potential of 0.5 a.u. At the largest distance of 50 a.u., the potential between the projectile and the convoy electron was −53/50, i.e., ~ −1 a.u. The latter potential increased rapidly when decreasing the distance between the electron and the projectile. Consequently, even though the electron–electron interaction had an influence on the momentum distributions, it was not expected to largely affect the fundamental results, i.e., the presence of structures in momentum distributions at large values of $q_\perp$.

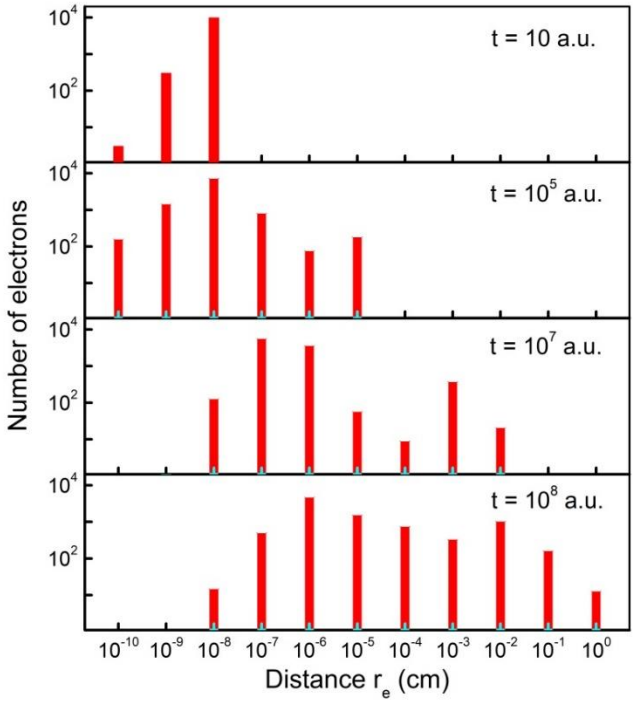

Figure 1. Convoy electron distributions at different times of a collision. The electrons move in the field of an Au^{53+} ion and the magnetic field B of 20 Gauss used in the experiment. Time t = 0 corresponds to a situation where the electrons are located at distances r_e smaller than 10^{-7} cm. As time increases, B deviates the electrons and the average r_e distance increases. At the end of the collision (bottom of Figure 1), most of the electrons can collide with the He target, since r_e is much smaller than 1 mm.

To go further with the analysis of SI in the present collision system, improvements of the previous model were performed. Instead of considering free electrons [13], Coulombic interactions between the convoy electrons and Au^{53+} were considered. Nevertheless, to simplify the problem, the interaction among these electrons was neglected. As discussed previously, the contribution of the magnetic field in the Hamilton equations was not considered, for reasons mentioned previously. To further elaborate on the hypothesis of convoy electrons, TDCS were also calculated and compared with existing experimental and theoretical results. The method used to calculate the DDCS and the TDCS is briefly described in the next section. The DDCS and the TDCS are presented in Sections 2.2 and 2.3, respectively. It will be shown that the agreement between our calculations and the experiment was remarkably good.

2. Results

2.1. CTMC Method

The multi-body classical trajectory Monte Carlo (MB-CTMC) method is based on a numerical solution of Hamilton's equations of motion for the many-body system, which includes the Au^{53+} and He^{2+} nuclei, as well as both He electrons and convoy electrons. The total Hamiltonian is $H_T = H_P + H_e$ where:

$$H_P = \sum_{k=1}^{4} \frac{p_k^2}{2m_k} + \sum_{k=1}^{3} \sum_{j=k+1}^{4} \frac{q_j q_k}{r_{jk}} + \sum_{i=1}^{2} \sum_{\beta=1}^{2} V_H^{\beta}\left(r_{\beta i}, p_{\beta i}\right) \quad (1)$$

and:

$$H_e = \sum_{i=1}^{N} \frac{p_i^2}{2} + \sum_{i=1}^{N} \sum_{j=1}^{2} \frac{1}{r_{ij}} - \sum_{i=1}^{N} \frac{53}{r_{iAu}} - \sum_{i=1}^{N} \frac{2}{r_{iHe}} \quad (2)$$

are the Hamiltonians describing the collision between Au^{53+} and He as well as between convoy electrons and the projectile and the target, respectively. More precisely, the first terms in Equations (1) and (2) are the kinetic energies of the four main particles (Au^{53+}, He^{2+} and both He electrons) and of the convoy electrons, respectively. The second term in Equation (1) is the potential energy between each of the four main particles cited above, and the three last terms in Equation (2) are the potential energies between each convoy electron and each He electron, (second term), the Au^{53+} nucleus (3rd term) and the He^{2+} nucleus (last term), respectively. The last term of Equation (1) is an additional phenomenological potential that ensures the stability of the He atom and will be described in detail below.

In Equation (1), $\vec{p_k}$, q_k and m_k are the momentum vector, the charge and the mass of particle k, respectively. The quantity r_{jk} is the distance between particles j and k, while r_{iAu} and r_{iHe} are the distances between one convoy electron and Au and He, respectively. In Equation (2), $\vec{p_i}$ is the momentum vector of one convoy electron.

The pseudo-potential $V_H^{\beta}\left(r_{\beta i}, p_{\beta i}\right)$, where β denotes each nucleus and i the index for each electron, was first introduced in nuclear physics [14] and then adapted for atomic structures [15] as well as ion–atom [16,17] and ion–molecule collisions [18]. Its expression is:

$$V_H^{\beta}\left(r_{\beta i}, p_{\beta i}\right) = \frac{\xi_H^2}{4\alpha\mu_\beta r_{\beta i}^2} exp\left[\alpha\left(1 - \left(\frac{r_{\beta i}\, p_{\beta i}}{\xi_H}\right)^4\right)\right] \quad (3)$$

where μ_β is the reduced mass between each nucleus and one He electron. The quantities $\xi_H = 0.9582$ and $\alpha = 4$ were chosen so that the first and second ionization potentials of He were close to the experimental ones [16]. With these values, the first and second ionization potentials of He were 1.1 a.u. and 2.3 a.u., respectively, which were quite close to the expected values of 0.9 a.u. and 2 a.u. The quantities $r_{\beta i}$ and $p_{\beta i}$ are the positions and momenta of He electrons, respectively, relative to the He nucleus or the Au nucleus.

Initially, the projectile was at a distance z_p = –200 a.u., and the orientation of the electron around the target was randomly chosen. The only initial constraints that insured the stability of the He atom were $\vec{r}_{He1} = -\vec{r}_{He2}$, and $\vec{p}_{He1} = -\vec{p}_{He2}$ [16], i.e., the electrons were diametrically opposite to each other and had opposite initial momenta to ensure that they moved in the same direction. The impact parameter b varied from 0 to 20 a.u. and the angle φ_p which characterized the position of the projectile in the (xOy) plane, was also randomly chosen. The initial spatial and momentum distributions were calculated using the method initiated previously by Abrines and Percival [19] and developed in several cases for the H target or multielectron targets (see for example [20]).

From the initial conditions, the Hamiltonian equations were numerically solved using the Runge–Kutta method of order 4, with an adaptive step defined and described in Ref. [19]. At the end of the collision, the number of projectiles that ionized one target electrons was determined as a function of the scattering angle θ_P, b and electron energy. During the simulation, we followed 5,000,000 primary trajectories.

2.2. Doubly Differential Cross Sections

Figures 2–4 show the projectile transverse momentum $q_\perp$ distributions for the emitted electron energies E_e of 10 eV, 50 eV, 90 eV and 130 eV when five, 50 and 200 convoy electrons were involved during the collision, respectively. The present calculations (red curves) were compared with the experimental DDCS (open circles) [3]. Firstly, we focused on Figure 2. When no convoy electrons were introduced (blue dashed curves), the binary peaks, that were located at $q_\perp$ larger than 1 a.u., were not reproduced by the 4B-CTMC calculations [13]. It should be noted that this result was similar to that observed in the calculations where the H target was used instead of the He target [21]. The introduction of only five convoy electrons already qualitatively improved the calculation, especially for small values of E_e. However, the number of convoy electrons was not enough to reproduce the maxima observed at large values of $q_\perp$.

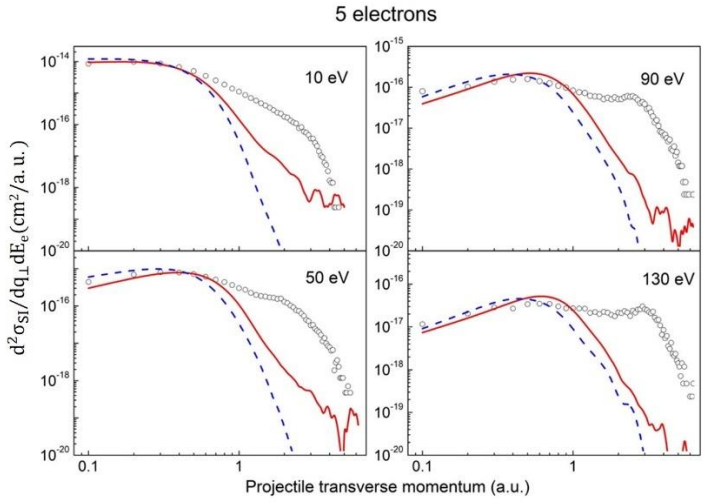

Figure 2. Doubly differential cross sections (DDCS) as a function of the projectile transverse momentum following the 3.6 MeV/amu Au^{53+} + He collisions, for the emission electron energies E_e = 10, 50, 90 and 130 eV. Open circles, experiment [3]; the dashed and full curves, the present multi-body classical Monte Carlo (MB-CTMC) model, convoluted with the experimental resolution of ~0.2 a.u.; the blue dashed curve, without the inclusion of the convoy electrons, and including 5 convoy electrons, red full curve.

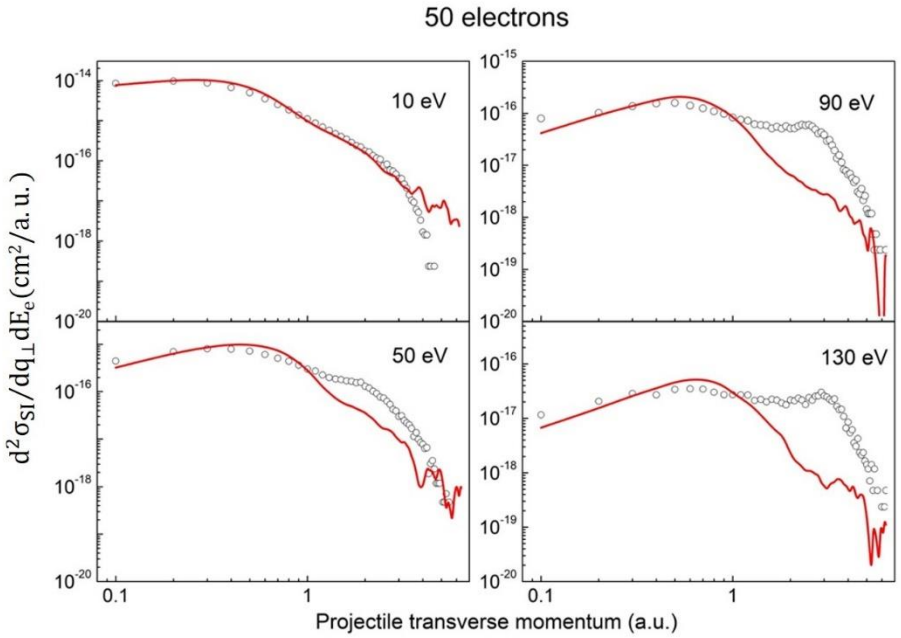

Figure 3. DDCS as a function of the projectile transverse momentum following the 3.6 MeV/amu Au^{53+} + He collisions, for the emission electron energies E_e = 10, 50, 90 and 130 eV. Open circles, experiment; the red full curves, the present MB-CTMC calculation with the inclusion of the 50 convoy electrons.

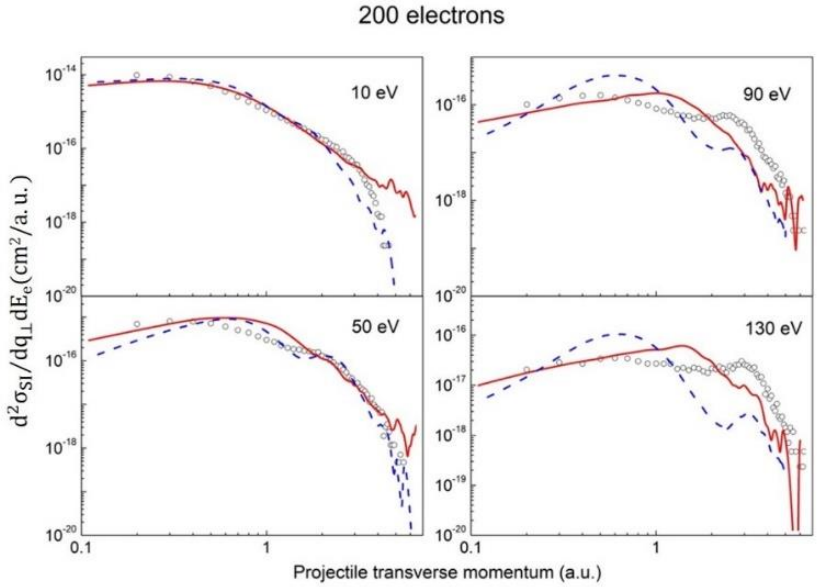

Figure 4. DDCS as a function of the projectile transverse momentum following the 3.6 MeV/amu Au^{53+} + He collisions, for the emission electron energies E_e = 10, 50, 90 and 130 eV. Open circles, experiment; the red full curves, the present MB-CTMC calculation with the inclusion of 200 convoy electrons that interact with the projectile; the blue dashed curves, recent four-body classical trajectory Monte Carlo (4B-CTMC) calculations [13] using 200 free electrons.

When multiplying the number of convoy electrons by a factor of 10 (see Figure 3), the improvement was remarkable for E_e = 10 eV, and clear maxima appeared at larger energies. However, quantitative discrepancies remained, especially for E_e = 90 and 130 eV. The good agreement observed at this emitted electron energy could be explained as follows: small values of E_e correspond to large impact parameters (of the order of 7 a.u.). In contrast, the impact parameters involved in the SI of He by

the electron impact were smaller than 2 a.u. For this reason, at small E_e, only the electrons that were located far from the projectile axis were efficient in ionizing the He target.

Finally, we focused on Figure 4, that represents the DDCS when the 200 convoy electrons were introduced. The present results were denoted by red curves, while the dashed blue curves were the previous results of the 4B-CTMC calculations when the convoy electrons were considered to be free (no interaction with Au^{53+}). At E_e = 10 eV and 50 eV, present theoretical cross sections were in very good agreement with the experiment and our previous calculations, except for $q_\perp$ larger than 3 a.u. At E_e = 90 eV and 130 eV, the agreement with experiment was quantitatively reasonable, and the present results were much better that those obtained with the free electrons. The discrepancies observed around $q_\perp$ = 1 a.u. may have several reasons: (i) the CTMC calculations were not well adapted to reproduce the experimental cross sections when the electron projectiles were involved during a collision (see for example Ref. [22]); (ii) it must be recalled that the initial distribution in space and in momentum of the convoy electrons may have influenced the results; (iii) the interaction between the convoy electrons, that was neglected in the present work, may have also changed the $q_\perp$ distribution.

2.3. Triply Differential Cross Sections

The TDCS measurements and calculations presented a substantial challenge, as they can show up significant discrepancies which can be hidden in less differential cross sections. In the case of the Au^{53+} + He collisions, as mentioned in the introduction, none of the theoretical interpretations of the experimental results [8] were satisfactory. As shown in Figure 5, the experimental TDCS for E_e = 4 eV and $q_\perp$ = 0.65 a.u. (open circles and black line) presented a maximum at an emitted electron angle θ_e around 0°. Among all the previous calculations, only a few theoretical results (see [23] and references inside) were shown (blue curves on top of Figure 5). First Born approximation, two-Coulomb wave model, three distorted-wave and three distorted-wave–eikonal-initial-state calculations gave rise to two structures, with a maximum at angles larger than 45°. On the contrary, the continuum-distorted-wave–eikonal-initial-state calculation [10] produced a wide structure whose maximum was located at about −50°.

The results of the present calculations are presented on the bottom of Figure 5, for 0, 10 and 20 convoy electrons (blue short dashed curve, blue dashed curve and red full curve, respectively). The region of integration for the angle was 10 degrees, and the energy region was, like in the experiment, 2 eV for the emitted electron energies E_e = 100 eV and 5 eV for E_e = 130 eV. The electron yield from our calculations was normalized to that obtained experimentally. Without any convoy electrons, the structure (blue short curve) had a maximum at ~ –50°, and no electron was emitted at angles larger than 100°. For 10 and 20 convoy electrons the structures were shifted to larger angles than those for no convoy electrons and presented a maximum at ~ 0°. It was also remarkable that the widths of the calculated structures reproduced quite well the experimental width. From this result, it appeared that the hypothesis of the presence of convoy electrons that actively participated to the collision can be considered as justifiable.

To confirm the validity of our hypothesis, similarly calculated TDCSs were extracted using 20 convoy electrons (red curves in Figure 6) for E_e = 4 eV and $q_\perp$ = 1 a.u. (Figure 6a), E_e = 10 eV and $q_\perp$ = 0.65 a.u. (Figure 6b) and E_e = 10 eV and $q_\perp$ = 1 a.u. (Figure 6c), for which experimental TDCSs were available (open circles). Again, the calculated structures, in contrast with previous calculations, were very close to the experimental results. The maxima were peaked at ~0° and the widths were very close to those observed experimentally. For small values of emitted electron energies and relatively large values of $q_\perp$, the number of convoy electrons was of the order of 20, while the total number of convoy electrons was of the order of 200. As mentioned earlier, this was due to the fact that a small energy of the emitted electron energy corresponds to relatively large impact parameters, so that only the convoy electrons that were located far from the projectile axis contributed to the He ionization.

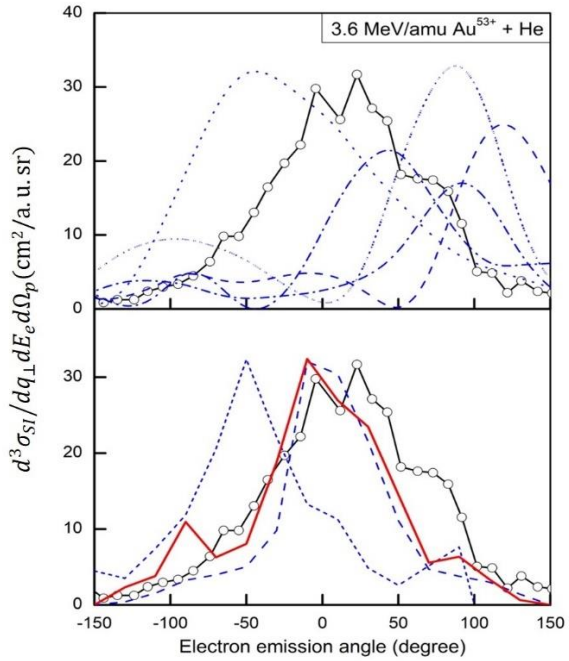

Figure 5. Triply differential cross sections (TDCS) as a function of the emitted electron angle following the 3.6 MeV/amu Au^{53+} + He collisions, for E_e = 4 eV and $q_\perp$ = 0.65 a.u. Open Circles, experiment [7]; top of Figure 5: the blue curves, previous theoretical calculations (see [22] and references therein); bottom of Figure 5: the blue short-dashed curve, blue dashed curve and red full curve, the present MB-CTMC calculation with 0, 10 and 20 convoy electrons, respectively.

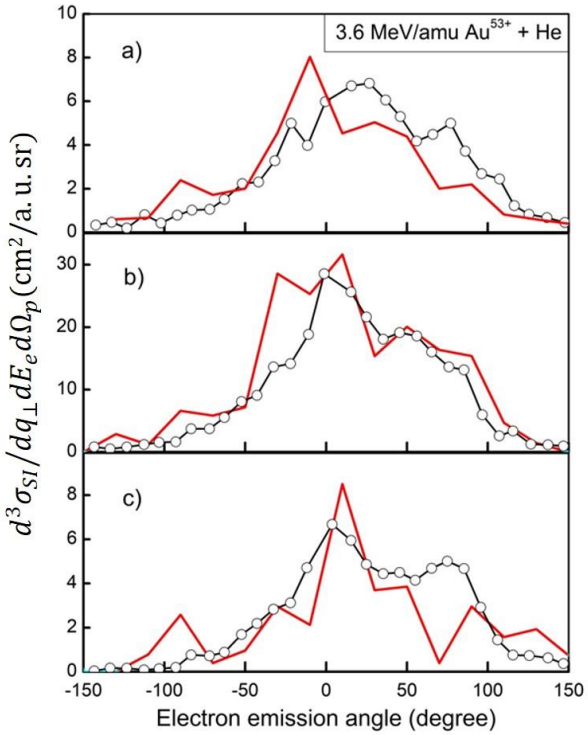

Figure 6. TDCS as a function of the emitted electron angle following the 3.6 MeV/amu Au^{53+} + He collisions, for (**a**) E_e = 4 eV and $q_\perp$ = 1 a.u., (**b**) E_e = 10 eV and $q_\perp$ = 0.65 a.u., (**c**) E_e = 10 eV and $q_\perp$ = 1 a.u. Open circles, experiment [7]; red curves, present calculations including 20 convoy electrons.

3. Conclusions

The DDCS and the TDCS following the single ionization of He by Au^{53+} ions at a projectile energy of 3.6 MeV/amu were revisited using the MB-CTMC method and compared with previous experiments. In addition to the Au^{53+} projectiles, the convoy electrons originating from the collisions with surfaces and emitted in the same direction as the incident projectile were included in the present calculation. In contrast with recent 4B-CTMC calculations [13], where free electrons were considered, the convoy electrons interacted with the projectile. The agreement with the experiment was found to be good, since the binary contributions observed experimentally were reproduced by the present model. To validate the hypothesis of the presence of convoy electrons during the collision, the TDCSs were also calculated and compared with previous measurements and theoretical calculations. The agreement between our MB-CTMC calculation and the experiment was found to be rather good and tends to confirm the necessity of introducing electrons originating from primary collisions following the projectile with nearly the same velocity. As mentioned by previous authors in their conclusions [2], we also suggest new experiments in which possible convoy electrons, if they exist, are removed without any ambiguity. Moreover, more sophisticated calculations would be desirable, in which the magnetic field would be introduced, as well as interactions between convoy electrons. In addition, a discussion concerning the dependence of the results upon the conditions of creation of convoy electrons would be necessary.

Funding: This research received no external funding

Acknowledgments: The author gratefully acknowledges M.S., R.M. and O.F. for fruitful discussions.

Conflicts of Interest: The author declares no conflict of interest

References

1. Olson, R.E.; Fiol, J. Mapping of the Bethe surface in single-ionization ion-atom collisions. *J. Phys. B At. Mol. Phys.* **2001**, *34*, L625. [CrossRef]
2. Fiol, J.; Olson, R.E. Three-and four-body dynamics in fast heavy ion–atom ionization. *J. Phys. B At. Mol. Phys.* **2004**, *37*, 3947. [CrossRef]
3. Moshammer, R.; Perumal, A.N.; Schulz, M.; Rodriguez, V.D.; Kollmus, H.; Mann, R.; Hagmann, S.; Ullrich, J. Three-body Coulomb problem probed by mapping the Bethe surface in ionizing ion-atom collisions. *Phys. Rev. Lett.* **2001**, *87*, 223201. [CrossRef] [PubMed]
4. Rodriguez, V.D. CDW-EIS theoretical calculations of projectile deflection for single ionization in highly charged ion–atom collisions. *Nucl. Instr. Methods Phys. Res. B* **2003**, *205*, 498. [CrossRef]
5. Fainstein, P.D.; Gulyás, L. Three-and four-body dynamics in single ionization of He by swift highly charged Au^{53+} ions. *J. Phys. B At. Mol. Phys.* **2005**, *38*, 317. [CrossRef]
6. Schulz, M.; Moshammer, R.; Perumal, A.N.; Ullrich, J. Triply differential single-ionization cross sections in fast ion-atom collisions at large perturbation. *J. Phys. B At. Mol. Phys.* **2002**, *35*, L161. [CrossRef]
7. Fischer, D.; Moshammer, R.; Schulz, M.; Voitkiv, A.; Ullrich, J. Fully differential cross sections for the single ionization of helium by ion impact. *J. Phys. B At. Mol. Phys.* **2003**, *36*, 3555. [CrossRef]
8. Foster, M.; Madison, D.H.; Peacher, J.L.; Ullrich, J. Highly charged particle impact ionization of He. *J. Phys. B At. Mol. Phys.* **2004**, *37*, 3797. [CrossRef]
9. Olson, R.E.; Fiol, J. Extreme sensitivity of differential momentum transfer cross sections to target atom initial conditions. *Phys. Rev. Lett.* **2005**, *95*, 263203. [CrossRef]
10. Ciappina, M.F.; Cravero, W.R. Post–prior discrepancies in CDW–EIS calculations for ion impact ionization fully differential cross sections. *J. Phys. B At. Mol. Phys.* **2006**, *39*, 1091. [CrossRef]
11. McGovern, M.; Assafrão, D.; Mohallem, J.R.; Whelan, C.T.; Walters, H.R.J. Coincidence studies of He ionized by C^{6+}, Au^{24+}, and Au^{53+}. *Phys. Rev. A* **2010**, *81*, 042704. [CrossRef]
12. Dürr, M.; Najjari, B.; Schulz, M.; Dorn, A.; Moshammer, R.; Voitkiv, A.B.; Ullrich, J. Analysis of experimental data for ion-impact single ionization of helium with Monte Carlo event generators based on quantum theory. *Phys. Rev. A* **2007**, *75*, 062708. [CrossRef]
13. Frémont, F. Transverse Momentum Transfer Distributions Following Single Ionization in 3.6 MeV/amu Au^{53++} He Collisions: A 4-Body Classical Treatment. *Atoms* **2018**, *6*, 68. [CrossRef]

14. Kirschbaum, C.L.; Wilets, L. Classical many-body model for atomic collisions incorporating the Heisenberg and Pauli principles. *Phys. Rev. A* **1980**, *21*, 834. [CrossRef]
15. Cohen, J.S. Quasiclassical effective Hamiltonian structure of atoms with Z=1 to 38. *Phys. Rev. A* **1995**, *51*, 266. [CrossRef]
16. Cohen, J.S. Quasiclassical-trajectory Monte Carlo methods for collisions with two-electron atoms. *Phys. Rev. A* **1996**, *54*, 573. [CrossRef]
17. Frémont, F.; Belyaev, A.K. Excitation of hydrogen atoms in collisions with helium atoms: The role of electron–electron interaction. *J. Phys. B At. Mol. Phys.* **2017**, *50*, 045201. [CrossRef]
18. Cohen, J.S. Molecular effects on antiproton capture by H2 and the states of $p^{-}p$ formed. *Phys. Rev. A* **1996**, *56*, 3583. [CrossRef]
19. Abrines, R.; Percival, I. Classical theory of charge transfer and ionization of hydrogen atoms by protons. *Proc. Phys. Soc.* **1966**, *88*, 861. [CrossRef]
20. Frémont, F. Electron capture and single ionization in H++ Ar collisions: Classical calculations. *J. Phys. B At. Mol. Phys.* **2016**, *49*, 065206. [CrossRef]
21. Fiol, J.; Olson, R.E. Three-body dynamics in hydrogen ionization by fast highly charged particles. *J. Phys. B At. Mol. Phys.* **2002**, *35*, 1759. [CrossRef]
22. Griffin, D.C.; Ballance, C.P.; Pindzola, M.S.; Robicheaux, F.; Loch, S.D.; Ludlow, J.A.; Witthoeft, M.C.; Colgan, J.; Fontes, C.J.; Schultz, D.R. The validity of classical trajectory and perturbative quantal methods for electron-impact ionization from excited states in H-like ions. *J. Phys. B At. Mol. Phys.* **2005**, *38*, L199. [CrossRef]
23. Feng, L.L.; Sun, S.Y.; Duan, Q.Q.; Jia, X.F. Fully Differential Cross Sections for Single Ionization of Helium by Au^{Q+} Impact. *Chin. J. of Chem. Phys.* **2015**, *28*, 595. [CrossRef]